Biol. Cybern. 92, 61–70 (2005)
DOI 10.1007/s00422-004-0522-2

Biological Cybernetics

A computational model of monkey cortical grating cells

Tino Lourens[1], **Emilia Barakova**[2], **Hiroshi G. Okuno**[1,3], **Hiroshi Tsujino**[1]

[1] Honda Research Institute Japan Co. Ltd., 8-1 Honcho, Wako-shi, Saitama, 351-0114, Japan
[2] Brain Science Institute, RIKEN 2-1 Hirosawa, Wako-shi, Saitama, 351-0198, Japan
[3] Graduate School of Informatics, Kyoto University Yoshida-Hommachi, Sakyo, Kyoto, 606-8501, Japan

Received: 20 April 2004 / Accepted: 13 September 2004 / Published online: 13 December 2004

Abstract. Grating cells were discovered in the V1 and V2 areas of the monkey visual cortex by von der Heydt et al. (1992). These cells responded vigorously to grating patterns of appropriate orientation and periodicity. Computational models inspired by these findings were used as texture operator (Kruizinga and Petkov 1995, 1999; Petkov and Kruizinga 1997) and for the emergence and self-organization of grating cells (Brunner et al. 1998; Bauer et al. 1999). The aim of this paper is to create a grating cell operator $\mathcal{G}$ that demonstrates similar responses to monkey grating cells by applying operator $\mathcal{G}$ to the same stimuli as in the experiments carried out by von der Heydt et al. (1992). Operator $\mathcal{G}$ will be tested on images that contain periodic patterns as suggested by De Valois and De Valois (1988). In order to learn more about the role of grating cells in natural vision, operator $\mathcal{G}$ is applied to 338 real-world images of textures obtained from three different databases. The results suggest that grating cells respond strongly to regular alternating periodic patterns of a certain orientation. Such patterns are common in images of human-made structures, like buildings, fabrics, and tiles, and to regular natural periodic patterns, which are relatively rare in nature.

1 Introduction

With their discovery of orientation-selective cells in primary visual cortex (simple and complex cells), Hubel and Wiesel (1962, 1974) triggered a wave of research activities in neurophysiology. These activities were aimed at a quantitative description of the functional properties of these cells (for reviews see De Valois et al. 1978, 1979; Albrecht et al. 1980; von der Heydt 1987). Computational models of simple cells using linear filters, in particular Gabor filters (Daugman 1985; Jones and Palmer 1987), followed by half-wave rectification are widely applied (Movshon et al. 1978; Andrews and Pollen 1979). Complex cell models require an additional step in processing, namely, spatial summation. Morrone and Burr (1988) modeled this summation by taking the amplitude of the complex values of the simple cell operator. Simple and complex cells respond to periodic stimuli and aperiodic stimuli such as sine- and square-wave grating, bars, and edges of a preferred orientation.

A decade ago, von der Heydt et al. (1991, 1992) reported the discovery of a new type of cell in areas V1 and V2 of the monkey visual cortex that responded to periodic stimuli. They called these cells "grating cells" because they responded vigorously to periodic patterns and only weakly or not at all to aperiodic patterns like bars or edges. They estimated that these cells make up around 4 and 1.6% of the population of cells in areas V1 and V2, respectively, and that in V1 around 4 million of these cells subserve the central 4° of visual field. Grating cells prefer spatial frequencies between 2.6 and 19 cycles per degree with tuning widths at half-amplitude between 0.4 and 1.4 octaves. They found that these cells are highly selective for the orientation of gratings and the number of cycles included. A minimum of 2–6 cycles was required to evoke a response, which then leveled off at 4–14 cycles (median 7.5). In this study we propose a computational model of grating cells that reproduces these measurements.

However, having obtained a model that can reproduce these measurements, the question arises as to whether these operators also respond to real-world patterns and, if so, to what kind? This question is important with regard to embedding the model into an artificial vision system.

This paper is organized as follows. In Sect. 2 computational models of simple and complex cells as known from the literature will be introduced and those used to develop the new grating cell operator will be described. In Sect. 3 the new grating operator will be constructed and divided into two classes, the first sensitive to achromatic and the second sensitive to chromatic stimuli. Cortical cells with functions equivalent to the latter type have not been described [since stimuli used by von der Heydt et al. (1992) were achromatic] but are likely to exist, since cortical areas V1 and V2 are quite responsive to chromatic stimuli (Engel et al. 1997). In Sect. 4, the output of operator $\mathcal{G}$ and the responses of grating cells will be compared by using the

Correspondence to: T. Lourens
(e-mail: tino@jp.honda-ri.com)

same type of stimuli as used by von der Heydt et al. (1992). In addition the output of the grating operator proposed by Kruizinga and Petkov (1995) is used for comparison. In Sect. 5 operator $\mathcal{G}$ will be applied to real-world images in order to obtain better insight into the function of grating cells in everyday vision. In Sect. 6 conclusions will be given.

2 Simple and complex cell operators

The receptive fields of simple cells can be modeled by complex-valued Gabor functions:

$$\hat{G}_{\sigma,\lambda,\gamma,\theta}(x,y) = \exp\left(i\frac{\pi x_1}{\sqrt{2}\sigma\lambda}\right)\exp\left(-\frac{x_1^2+\gamma^2 y_1^2}{2\sigma^2}\right), \quad (1)$$

where $x_1 = x\cos\theta + y\sin\theta$ and $y_1 = y\cos\theta - x\sin\theta$. Parameters σ, λ, γ, and θ represent scale, wavelength, spatial aspect ratio, and orientation, respectively.[1] These Gabor functions have been modified such that their integral vanishes and their one-norm (the integral over the absolute value) becomes independent of σ, resulting in $G_{\sigma,\lambda,\gamma,\theta}(x,y) = \eta\hat{G}_{\sigma,\lambda,\gamma,\theta}(x,y)$, where $\eta = \eta^{+}_{\mathrm{Re}}$ for the positive-valued real part of $\hat{G}$, $\eta = \eta^{-}_{\mathrm{Re}}$ for the negative-valued real part of $\hat{G}$, and $\eta = \eta_{\mathrm{Im}}$ for the imaginary part of $\hat{G}$. For details about these constants see Lourens (1998). A spatial convolution was used to transform input image $I(x,y)$ by these operators to yield the simple cell operator, and the amplitude of the complex values (Morrone and Burr 1988)

$$\mathcal{C}_{\sigma,\lambda,\gamma,\theta} = \left|\left|I * G_{\sigma,\lambda,\gamma,\theta}\right|\right| \quad (2)$$

was taken to obtain the complex cell operator. This operator formed the basis of the grating cell operator $\mathcal{G}$ to be described later in this paper. A high value at a certain combination of (x,y) and θ represents evidence for a contour element (bar or edge) oriented orthogonally to θ. Orientations are sampled linearly $\theta_i = i\pi/N, i = 0,\ldots,N-1$, and the scales are sampled $\sigma_j = \sigma_{j-2} + \sigma_{j-1}$, for $j = 2\ldots S-1$, where σ_0 and σ_1 represent constants.

3 Grating cells

Von der Heydt et al. (1991) proposed a model of grating cells in which the activities of displaced semilinear units of the simple cell type are combined by an AND-type nonlinearity to produce grating cell responses. This model responds properly to gratings of appropriate orientation and not to single bars and edges. However, the model does not account for correct spatial frequency tuning (the model also responds to all multiples of the preferred frequency) and responds to, for instance, a bar and an edge stimulus to which a grating cell would not respond (Petkov and Kruizinga 1997).

[1] The used Gabor function is similar to the one used by Petkov and Kruizinga (1997) when $\xi = \eta = \varphi = 0$ and spatial frequency $1/(2\sqrt{2}\sigma\lambda)$ are used.

Kruizinga and Petkov (1995) and Petkov and Kruizinga (1997) aimed at a model that reproduces the properties known from neurophysiological experiments and proposed a grating cell operator that was based on units comparable to simple cell with symmetrical receptive fields. The responses of these operators were evaluated along a line segment by a maximum operator M. A quantity q, which is 0 or 1, was used to compensate for contrast differences, and a point spread function was used to meet the spatial summing properties with respect to the number of bars and length. Except in its spatial summation properties, this operator differs from the grating cell responses, and it does not always account for correct spatial frequency tuning; it is unable to discriminate between alternating light and dark bars of preferred width and alternating bars of about three times this preferred width. The origin of this artifact and how it can be avoided will be demonstrated in this paper.

In this paper, we present an operator $\mathcal{G}$ that meets the response profiles of the cortical grating cells and their appropriate frequency tuning. This operator uses the output complex cell operators as described in (2). As in the other models, we evaluate (along a straight line) the responses of these operators orthogonal to the length of the bars of a grating. Let us denote the length of the evaluation the "evaluation-length." Unlike the other models, we let the evaluation-length of the evaluation depend on the similarity of the responses of the complex cells, but this evaluation-length is at least $2B_{\min}$ and at most $2B_{\max}$ bars. Instead of a maximum operator, we use an averaging operator. No contrast normalization mechanism is incorporated into the grating operator since we believe that this is compensated for at the stage of the center-surround cells in the retina; see, e.g., Kaplan and Shapley (1986). This implies that the input data are already normalized for contrast.

3.1 Grating cell operator

The complex cell operator responds vigorously and uniformly to grating patterns of a preferred frequency. Its response decreases and becomes less uniform when applied to grating patterns of a different frequency (see Fig. 3 (C response for $\lambda = 1.00$) for a one 1D example). These response strengths together with the uniformity of these responses, which are measured along a line perpendicular to the orientation of the bars, are used to construct the initial grating response

$$\mathbf{G}_{\sigma,\lambda,\gamma,\theta,l}(x,y) = \frac{\rho}{2l+1}\sum_{i=-l}^{l}\mathcal{C}_{\sigma,\lambda,\gamma,\theta}(x+x_i, y+y_i), \quad (3)$$

where ρ is a response decrease factor. This factor is a measure of the deviation from the optimal spatial frequency and uniformity of the complex cell responses. It will be discussed below. The evaluation-length, which equals $2l$, is the length over which summation of the complex operator will take place.

Since these operations are performed on a discrete grid, we decompose the maximum length from the center of the line segment, in x- and y-directions:

$$l_x = B_{\max}\sqrt{2}\sigma\lambda\cos\theta \quad \text{and} \quad l_y = B_{\max}\sqrt{2}\sigma\lambda\sin\theta\,. \tag{4}$$

Similarly, we decompose the minimum length ($B_{\min}$) into m_x and m_y. The preferred bar width (in pixels) equals $\sqrt{2}\sigma\lambda$.

Depending on the preferred orientation θ, the evaluation will take place in the x- or y-direction. Hence, parameters x_i, y_i, $l_{\min}$, and $l_{\max}$ are orientation dependent:

$$\begin{aligned}
&\textbf{if}\left(\left|\frac{l_y}{l_x}\right| \le 1 \quad \text{and} \quad l_x \neq 0\right)\\
&\textbf{then}\\
&x_i = i;\; y_i = \left\lfloor i\frac{l_y}{l_x} + 0.5 \right\rfloor;\\
&l_{\max} = |\lfloor l_x + 0.5\rfloor|;\; l_{\min} = |\lfloor m_x + 0.5\rfloor|\\
&\textbf{else}\\
&x_i = \left\lfloor i\frac{l_x}{l_y} + 0.5 \right\rfloor;\; y_i = i;\\
&l_{\max} = |\lfloor l_y + 0.5\rfloor|;\; l_{\min} = |\lfloor m_y + 0.5\rfloor|\,,
\end{aligned} \tag{5}$$

where $\lfloor x\rfloor$ denotes the floor function, i.e., the nearest integer value smaller than or equal to x. The evaluation-length parameter l of (3) is determined by the maximum, minimum, and average response of the complex cell operator along a straight line:

$$\begin{aligned}
&l = \min_i(l_i); \quad l_{\min} < i \le l_{\max};\\
&\textbf{if}\left(\frac{\mathbf{G}^{\max}_{\sigma,\lambda,\gamma,\theta,i}(x,y) - \mathbf{G}^{\text{avg}}_{\sigma,\lambda,\gamma,\theta,i}(x,y)}{\mathbf{G}^{\text{avg}}_{\sigma,\lambda,\gamma,\theta,i}(x,y)} \ge \Delta \vee \right.\\
&\left.\frac{\mathbf{G}^{\text{avg}}_{\sigma,\lambda,\gamma,\theta,i}(x,y) - \mathbf{G}^{\min}_{\sigma,\lambda,\gamma,\theta,i}(x,y)}{\mathbf{G}^{\text{avg}}_{\sigma,\lambda,\gamma,\theta,i}(x,y)} \ge \Delta\right)\\
&\textbf{then}\\
&l_i = i - 1\\
&\textbf{else}\\
&l_i = l_{\max}\,,
\end{aligned} \tag{6}$$

where $i \in \mathbb{Z}$ and constant $\Delta > 0$ is a uniformity measure. We used $\Delta = 0.25$ in all experiments. The minimum, maximum, and average $\mathbf{G}$ responses are obtained as follows:

$$\mathbf{G}^{\Omega}_{\sigma,\lambda,\gamma,\theta,l}(x,y) = \Omega^{l}_{i=-l}\left(\mathcal{C}_{\sigma,\lambda,\gamma,\theta}(x+x_i, y+y_i)\right)\,, \tag{7}$$

where Ω denotes the min, max, or avg operator.

The determination of the evaluation-length parameter l depends on the uniformity of responses of the complex cell operator along a line orthogonal to orientation θ. However, the evaluation length would have no impact on the response of the $\mathbf{G}^{\text{avg}}$ operator of (7). In (3), therefore, a response decrease factor $\rho = \rho_l\rho_u$ that is decomposed into a length evaluation and a uniformity decrease factor has been introduced. The decrease factor for the evaluation length

$$\rho_l = \frac{l/l_{\max}B_{\max} - B_{\min}}{B_{\max} - B_{\min}} = \frac{l - l_{\min}}{l_{\max} - l_{\min}} \tag{8}$$

is a linearly increasing response between $B_{\min}$ and $B_{\max}$. This ensures a strong decrease for short evaluation-lengths (it equals 0 for $l_{\min}$).

The uniformity decrease factor is measured by the deviation between the strongest and weakest response of the $\mathcal{C}$ operator along the evaluated line, when the evaluation length is larger than the minimum number of bars plus one (otherwise it is ignored, i.e., $\rho_u = 1$):

$$\begin{aligned}
&\textbf{if}\,(l_s \le l_{\min})\\
&\textbf{then}\\
&\rho_u = 1\\
&\textbf{else}\\
&\rho_u = 1 - \frac{\mathbf{G}^{\max}_{\sigma,\lambda,\gamma,\theta,l_s}(x,y) - \mathbf{G}^{\min}_{\sigma,\lambda,\gamma,\theta,l_s}(x,y)}{2\Delta\mathbf{G}^{\text{avg}}_{\sigma,\lambda,\gamma,\theta,l_s}(x,y)}\,,
\end{aligned} \tag{9}$$

where $l_s = l - l_{\max}/(1 + \lfloor B_{\max}\rfloor)$ is the length that is one bar shorter in evaluation-length parameter l. The slightly shorter evaluation-length ensures that both criteria in (6) are less than Δ, which implies that $\rho_u \ge 0$.

A weighted summation is made to model the spatial summation properties of grating cell operators with respect to the number of bars and their evaluation-length, which yields the grating cell response:

$$\mathcal{G}_{\sigma,\lambda,\gamma,\theta,\beta} = \mathbf{G}_{\sigma,\lambda,\gamma,\theta,l} * g_{\frac{\sigma\beta}{\lambda}}\,, \tag{10}$$

where $g_s(x,y) = 1/(2\pi s^2)\exp(-(x^2+y^2)/(2s^2))$ is a 2D Gaussian function. In combination with $B_{\min}$ and $B_{\max}$, parameter β determines the size of the area over which summation takes place. Parameters $B_{\min} = 0.5$ and $B_{\max} = 2.5$, together with a β between 2 and 4, yield good approximations of the spatial summation properties of cortical grating cells. In the experiments we used $\beta = 3$.

3.2 Color-opponent type of grating cells

Achromatic stimuli were used by von der Heydt et al. (1992); therefore they have not reported on the existence of color-opponent grating cells. However, evidence of other experiments suggest that such cells are plausible. Livingstone and Hubel (1984) already found opponent color-sensitive cells at the first level of processing after the photoreceptors. They found orientation-selective cells in area V1 that were color sensitive too. The receptive fields of these cells include elongated subregions that give excitatory responses to one color and inhibitory responses to another (opposite) color. The opponent color pairs were red-green and blue-yellow or vice versa. Cells of this type are found in area V4 (Zeki 1993) and in area V2, where 21–43% of the neurons have these properties (Gegenfurther et al. 1996; Tamura et al. 1996).

For modeling grating cells sensitive to chromatic stimuli, we used color-opponent complex cell operators (Würtz and Lourens 2000) defined as follows:

$$\mathcal{C}^{e,i}_{\sigma,\lambda,\gamma,\theta} = \left|\left|(I^e - I^i) * G_{\sigma,\lambda,\gamma,\theta}\right|\right|\,, \tag{11}$$

where $(e,i) \in \{(r,g),(b,y)\}$ is a red-green or a blue-yellow color-opponent pair.[2] Yellow is obtained by the average

[2] The order of a color pair is arbitrary since $\mathcal{C}^{e,i}_{\sigma,\lambda,\gamma,\theta} = \mathcal{C}^{i,e}_{\sigma,\lambda,\gamma,\theta}$.

of the red and green component: $y = (r + g)/2$, I^a denotes color channel $a \in \{r, g, b, y\}$ of image I.

In analogy to the initial achromatic grating cell operator of (3), the initial color-opponent grating cell operator should be modified to

$$\mathbf{G}^{e,i}_{\sigma,\lambda,\gamma,\theta,l}(x, y) = \frac{\rho^{e,i}}{2l^{e,i}+1} \sum_{j=-l^{e,i}}^{l^{e,i}} \mathcal{C}^{e,i}_{\sigma,\lambda,\gamma,\theta}(x + x_j, y + y_j), \quad (12)$$

where $l^{e,i}$ and $\rho^{e,i}$ are evaluated as before, but $\mathbf{G}^{\mathrm{avg},e,i}$ should be used instead of $\mathbf{G}^{\mathrm{avg}}$. Similarly, the $\mathbf{G}^{\min}$ and $\mathbf{G}^{\max}$ operators are evaluated by using antagonistic color channels.

The color-opponent grating cell operator, which is a modified version of the achromatic grating response from (10), is as follows:

$$\mathcal{G}^{e,i}_{\sigma,\lambda,\gamma,\theta,\beta} = \mathbf{G}^{e,i}_{\sigma,\lambda,\gamma,\theta,l} * g_{\frac{\sigma\beta}{\lambda}}. \quad (13)$$

The orientations of the grating cells are combined with an amplitude operator (for $\mathcal{G}$ also $\mathcal{G}^{e,i}$ can be substituted):

$$\mathcal{G}_{\sigma,\lambda,\gamma,\beta} = \sqrt{\sum_{j=0}^{N-1} \left(\mathcal{G}_{\sigma,\lambda,\gamma,\theta_j,\beta}\right)^2}, \quad (14)$$

where N denotes the number of orientations and $\theta_j = j\pi/N$. The achromatic and two color-opponent (red-green and blue-yellow) channels are combined by taking their maxima to yield the final grating cell operator

$$\mathcal{G}^{\mathrm{all}}_{\sigma,\lambda,\gamma,\beta} = \max\left(\mathcal{G}_{\sigma,\lambda,\gamma,\beta}\ ,\ \max_{(e,i)}\left(\mathcal{G}^{e,i}_{\sigma,\lambda,\gamma,\beta}\right)\right) \quad (15)$$

at a single scale. Since $\mathcal{C}^{e,i}_{\sigma} = \mathcal{C}^{i,e}_{\sigma}$, and hence also $\mathcal{G}^{e,i}_{\sigma,\lambda,\gamma,\theta,\beta} = \mathcal{G}^{i,e}_{\sigma,\lambda,\gamma,\theta,\beta}$, one channel for every opponent pair is sufficient. When an achromatic stimulus is applied to (15), it reduces to (10), because $\mathcal{G}^{e,i} = 0$ for both color-opponent channels.

4 Properties of grating cells

Von der Heydt et al. (1992) estimated several properties of grating cells. First, they determined their sensitivity to spatial frequency and orientation. Second, they used square-wave gratings to define the sensitivity of these cells to the number of bars included in the stimulus (spatial cycles). Third, they described the response of these cells to checkerboard patterns. Finally, they used the so-called Stresemann patterns (gratings in which every other bar was displaced by a fraction of a cycle). End-stopped grating cells that responded only at the end of a grating pattern were found as well, but they will not be considered in this study.

The contrast profiles of magno and parvo cells (Kaplan and Shapley 1986) show similarities with the profiles given by von der Heydt et al. (1992). In our model we assume that contrast normalization takes place. Hence, we did not simulate contrast sensitivity in this study.

The properties of the new grating cell operator will be evaluated by applying the operator to similar input stimuli (images). Parameters λ and γ are tuned to resemble the response profiles of the cortical grating cells. Then, these results will be compared with the measured data and the response properties of the model of Kruizinga and Petkov (1995) and Petkov and Kruizinga (1997).

4.1 Responses to test patterns

Figure 1 illustrates that the grating cell operator of (15) shows a behavior similar to that of the cortical grating cells. Grating cells responded vigorously to grating patterns of a certain orientation and spatial frequency, whereas small deviations to this pattern reduced this response.

4.2 Orientation and frequency profiles

In this section the properties of cortical grating cells will be modeled as accurately as possible by adjusting the parameters λ and γ of the defined operator. In the figures, these responses will be labeled using the settings of these parameters and those of the cortical cells by the expression "vdH . . . ."

The orientation bandwidth for grating cells is small; their half-maximum responses are at $\pm 6^\circ$. In the model this orientation tuning corresponded to $\lambda\gamma = 0.25$ and is illustrated in Fig. 2a.

Grating cells have different preferred frequency profiles. The response curves for, e.g., a low- and a high-bandwidth-sensitive cortical grating cell (Figs. 2b, c) were somewhat different. After having tested several combinations of parameters, $\lambda = 1.00$ and $\gamma = 0.25$ were found to most closely resemble the response profiles of low-spatial-frequency-sensitive cortical cells, while $\lambda = 0.33$ and $\gamma = 0.75$ most closely resembled the response profile of the high-spatial-frequency-sensitive cortical cells. Note that in both cases the orientation bandwidth ($\lambda\gamma = 0.25$) has been preserved.

However, a problem occurred when the setting of γ was approximately 0.4 or larger. At a spatial frequency that is a factor 3 lower than the preferred spatial frequency, the operator showed a "second" response profile with a local maximum response of 25% of the maximum response. This phenomenon is demonstrated in Figs. 2b, c, for 1–2 and 5–10 cycles per degree, respectively. The choice $\lambda = 1.00$ and $\gamma = 0.25$ avoids this artifact and is still an appropriate choice for high frequency sensitive cortical cells. For instance, if a preferred bar width of eight pixels corresponds to 19 cycles per degree, then the measured high-frequency bandwidth, which has a response of 50% or higher, would be between 6.6 and 8.9 pixels, while the modeled operator would have a bandwidth that is between 5.4 and 12.7 pixels.

In the simulations, the definition of the stimuli in terms of visual angle (cycles per degree) was arbitrary because

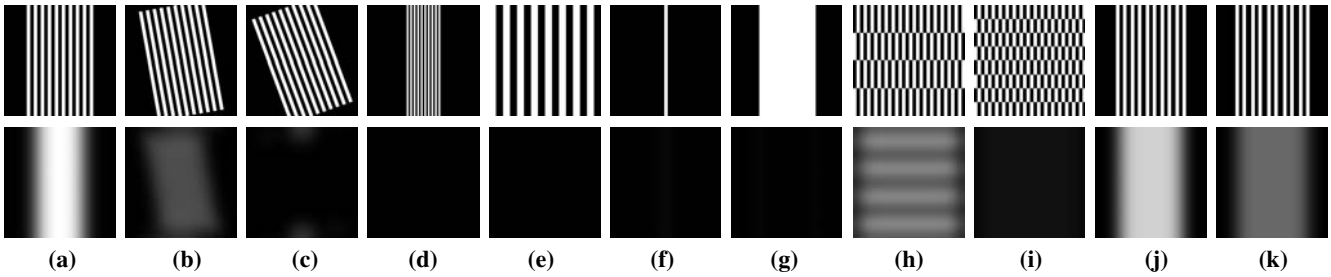

Fig. 1. Responses to square gratings of different orientations and spatial frequencies. *Top rows* show the stimulus and *bottom rows* the responses of the modeled grating operator. **a** Grating cells responded vigorously to grating patterns of preferred orientation and frequency. Responses decreased when the stimulus differed from this pattern. **b, c** Responses strongly decreased when the gratings were rotated by 10° and completely vanished at a 20° rotation. **d, e** Doubling or halving the spatial frequency also abolished these responses. **f, g** Grating cell operators did not respond to single bars or edges. **h, i** Checkerboard patterns also reduced the responses of these operators. **j, k** Stresemann patterns produced similar results. The settings of the parameters were $\lambda = 1.00$, $\gamma = 0.25$, $\beta = 3.00$, $B_{\min} = 0.5$, and $B_{\max} = 2.5$

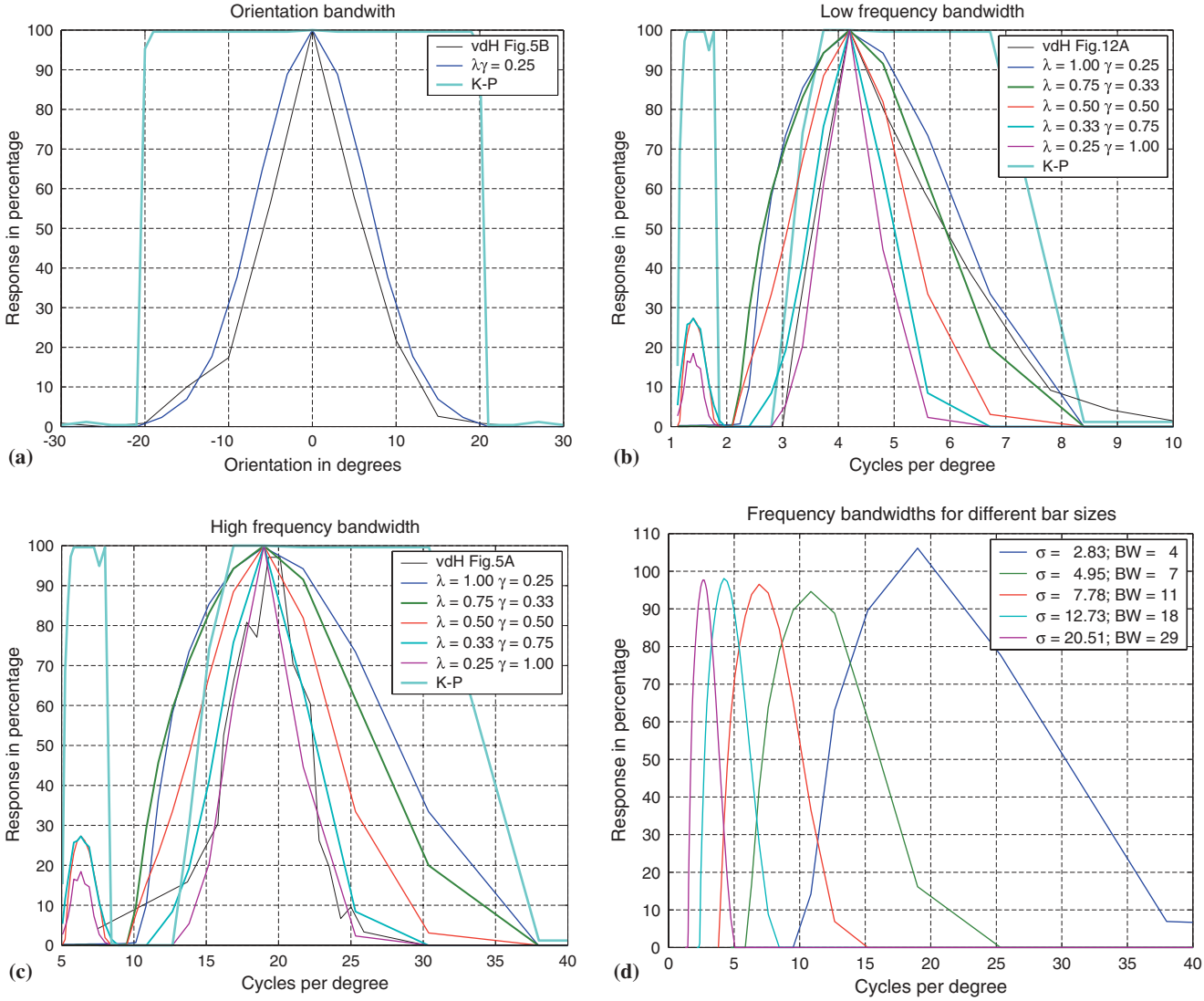

Fig. 2. Comparison of responses of cortical grating cells with the responses of grating cell operators. **a** Orientation. **b, c** Low-frequency and high-spatial-frequency profiles. **d** Spatial frequency profiles for different preferred bar width sizes (BW = 4, 7, 11, 18, and 29 pixels). Parameter settings: $\lambda = 1$ and $\gamma = 0.25$

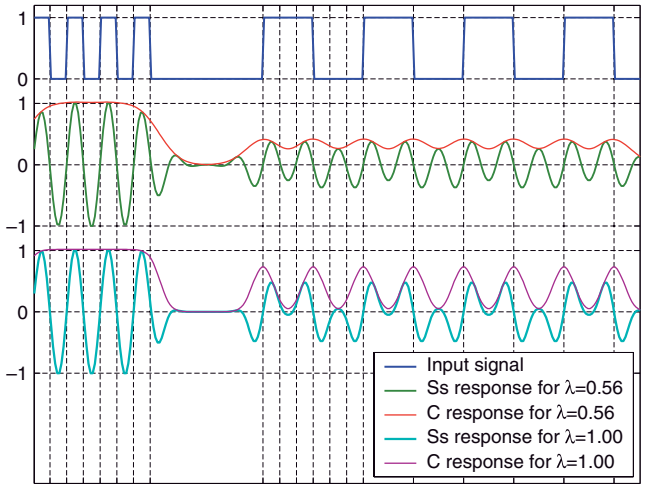

Fig. 3. Input signal (*top*). Response profile for symmetrical simple (*SS*) and complex (*C*) cell operators for $\lambda = 0.56$ (*middle*) and $\lambda = 1.00$ (*bottom*)

this is a biological measure depending on the distance between the observer and the stimulus. Hence, grating cell operators with a preferred bar width of eight pixels could correspond to both 4.2 and 19 cycles per degree. However, the response profiles for narrow bars demonstrate small differences. This is due to the discretization properties of the Gabor filters. Figure 2d illustrates that operators preferring small bar widths (four pixels or less) produced responses of over 100%. Also, in such a case, only seven measurements can be performed because the operator only responds to bar widths between one and seven pixels.

Figure 2d illustrates the bandwidths for operators preferring different bar widths (right to left: 4, 7, 11, 18, and 29 pixels, respectively). This figure illustrates that these five "scales" cover the full range of preferred frequencies (2.6 to 19 cycles per degree) assuming that a grating with a bar width of four pixels corresponds to a grating of 19 cycles per degree. If so, a grating of 2.6 cycles per degree would have a bar width of $4 \times 19/2.6 = 29.2$ pixels. Hence, these five scales cover well the range of cortical grating cells, considering that the drop in response strength between these five preferred frequencies drops at most 25% from the maximum response.

The grating cell operator of Kruizinga and Petkov (1995) and Petkov and Kruizinga (1997) is available online (http://www.cs.rug.nl/users/imaging/grcop.html) and was used with a bandwidth of 1.0 and a periodicity that equals two times the preferred bar width. The response profile (denoted by "K-P" in the figures) of this grating operator shows two global states, namely, inactivity or vigorous firing, caused by the built-in normalization quantity q. The choice of $\lambda = 0.56$ gives strong responses to two intervals (see Fig. 2b at 1–2 and 4–7 cycles per degree and Fig. 2c at 6–8 and 18–30 cycles per degree), which is caused by the simple cell operators. The higher spatial frequency curves are due to responses to the bars. The lower spatial frequency response curve is an artifact; it is due to an up-and-down going edge of a bar. In the middle of such a low-frequency bar there is still some response from both edges, causing a response profile that is similar to that of bars of the preferred frequency. An illustration of this behavior is given for a 1D signal in Fig. 3. This behavior does not occur for $\lambda = 1.00$, as is illustrated in the same figure, which motivates our choice for λ, for both lower and higher spatial frequencies.

4.3 Profiles for different textures

Figure 4a demonstrates the responses of three cortical grating cells to stimuli that include different numbers of bars. It shows that the responses of these cells increases with increasing numbers of bars. For comparison, the corresponding responses for the "K-P" operator are shown together with the responses of our operator, again set with different parameters. One can see that all responses were slightly different but nevertheless well within the range of cortical cells.

With regard to checkerboards, our operator was not as robust as the cortical cells (Fig. 4b) but showed a similar response profile when a checkerboard stimulus at different orientations was given (Fig. 4c). By contrast, the modeled cells are slightly less sensitive to shifts of bars (Fig. 4d). The responses to different orientations depended on the orientation bandwidth. With $\lambda\gamma = 0.25$ the orientation bandwidth was similar to that of the cortical cells, but the response was lower (by about three times) than the corresponding responses of cortical grating cells. On the other hand, with $\lambda\gamma = 0.35$ the responses were comparable, but the orientation bandwidth became wider than that of the cortical cells.

5 Examples of responses to oriented periodic patterns

The grating cell operator has been implemented in the visual programming environment TiViPE (Fig. 5a). In this figure, the "GratingResponses" icon performs (14) for the achromatic and two opponent-color channels separately. The two "DoubleOperand" icons perform the maximum operations as given in (15). The "Threshold" icon, with a thresholding value of 7, which avoids responses to noise, results in a binary response image. The "FeaturesOnImage" icon overlays these results (in red) on the monochromized input image. The same parameter settings were used for all experiments (Fig. 5b).

Most plants have highly repetitive patterns; the leaves of bushes, ferns, and trees tend to be numerous. De Valois and De Valois (1988) argued that a periodic pattern is easier for a plant to encode genetically because of its redundancy; for the same reason it should be easier for the visual system to decode such a pattern. The grating cell operator was applied to several naturally occurring periodic patterns of ferns, flowers, snakes, sand, and a few human-made periodicities (initially text of the manuscript and a ceiling) (Fig. 6). The grating cell operator showed weak or moderate responses to plants and animals. An exception was the strong response to the diamond python image (column 8 of Fig. 6), since its pattern closely resembles that

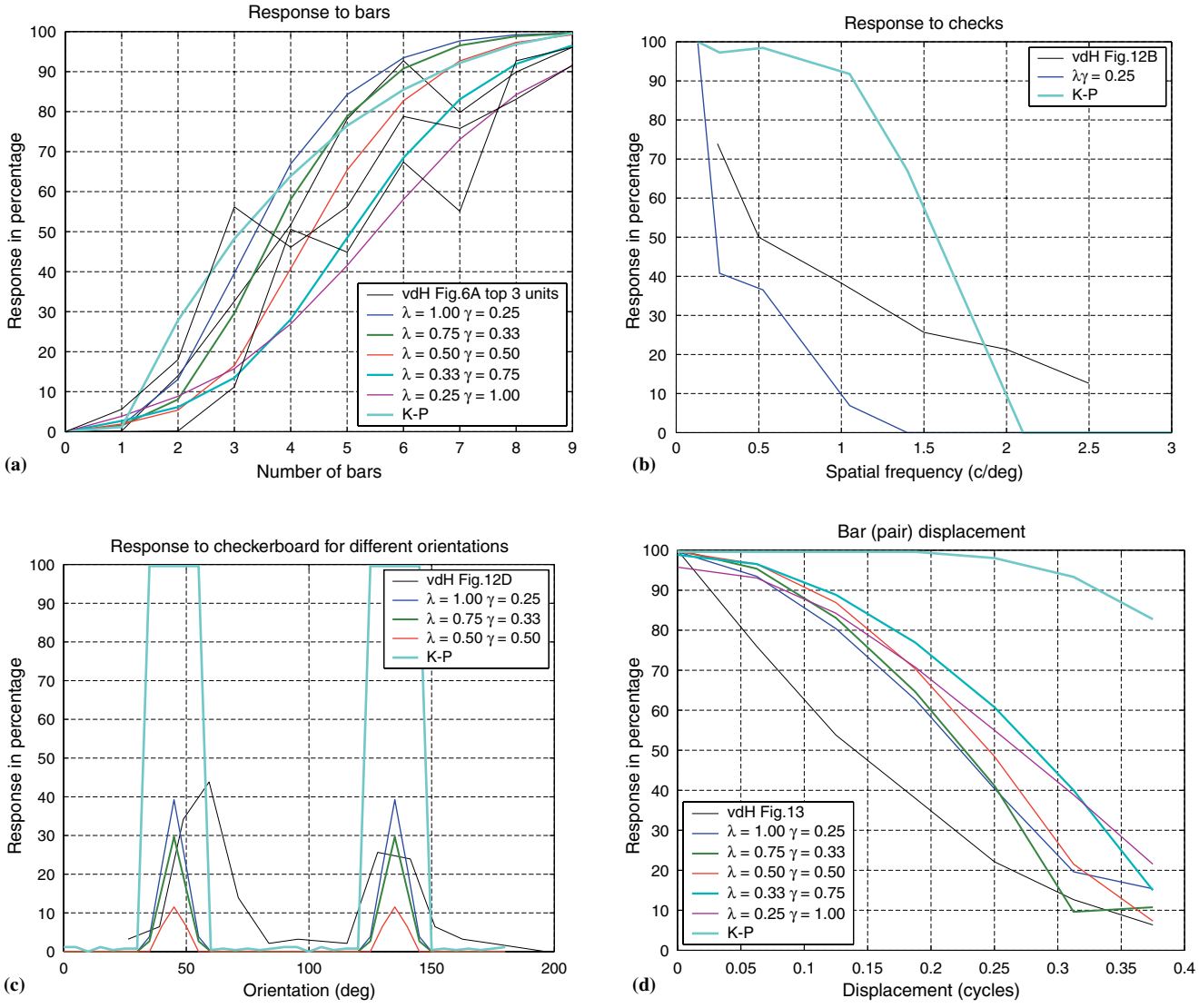

Fig. 4. Measured and modeled properties of grating cells. **a** Response profile for increasing number of bars. **b** Response to checks. **c** Sensitivity to different orientations of checkerboard patterns. **d** Responses to the so-called Stresemann pattern with increasing shift of bars

of a checkerboard. Response to sand patterns created by wind and water can be strong if the patterns are regular.

Responses to human-made periodic patterns such as a ceiling or printed text are strong. The accuracy of responses to the latter was striking, but details of marking text are beyond the scope of this paper. Many other images that contain natural periodic patterns of grass, plants, and flowers were applied, but the grating cell operator did not respond to those patterns. These findings suggest that grating cells do respond moderately to natural regular periodic patterns but strongly to the human-made periodicities.

The new operator has been applied to images containing textures, human-made (periodic) patterns inclusive, from three (Brodatz, ColumbiaUtrecht, and the VisTex) freely available databases. The Brodatz database contains 111 images D1 to D112, where D14 is missing. The central part (512×512 pixels) of the grayscale images that were sized 640×640 was used. The ColumbiaUtrecht database contains 61 images (sample 01 to sample 61). The central part (256×256 pixels) of the color images that are sized 640×480 was used. In the VisTex database 166 color images with a size of 512×512 pixels were used.

The grating cell operator was used with $N = 16$ orientations, which was necessary because the half-maximum response of the grating cells is at $\pm 6^\circ$ (see also Fig. 2a). Five different preferred spatial frequencies (scales) were used that cover the whole spectrum (2.6–19 cycles per degree) of cortical cells. These scales were combined using a maximum operator to yield one response per stimulus:

$$\mathcal{G}\mathrm{all}_{\lambda,\gamma,\beta} = \max_{i=0}^{S-1} \left(\mathcal{G}\mathrm{all}_{\sigma_i,\lambda,\gamma,\beta} \right) \quad , \tag{16}$$

where $S = 5$ is the number of scales and $\sigma_0 = 4\lambda/\sqrt{2}$, $\sigma_1 = 7\lambda/\sqrt{2}$, and $\sigma_j = \sigma_{j-2} + \sigma_{j-1}$ for $j \geq 2$ (as given earlier). The minimum bar width at σ_0 is 4, since smaller widths lead to strong inaccuracies due to the discreteness of the Gabor filters.

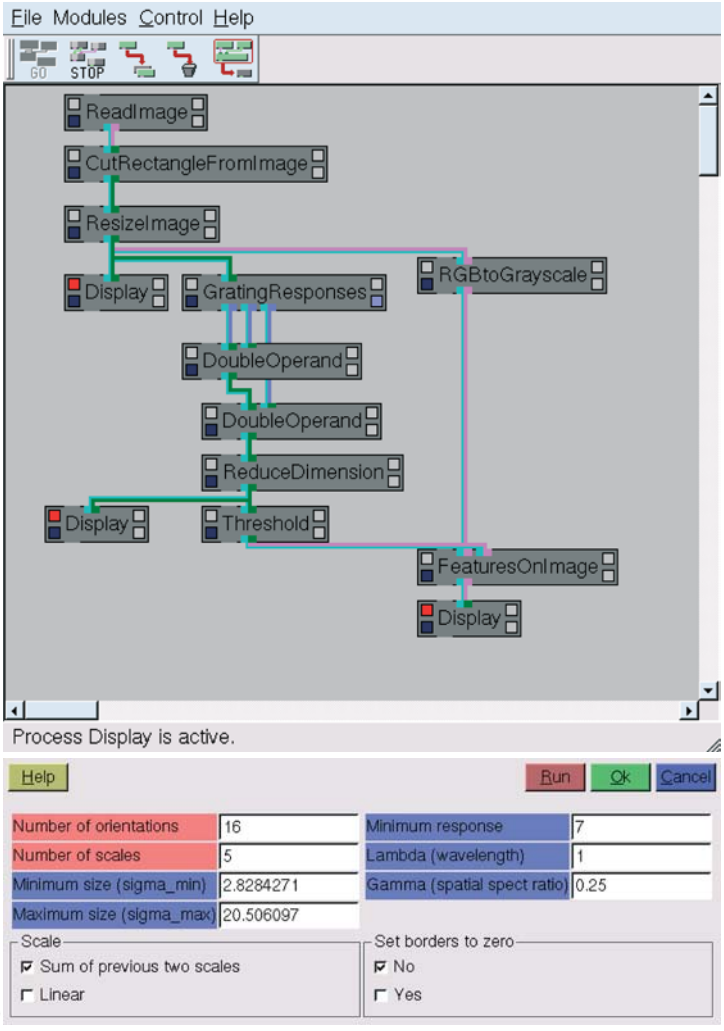

Fig. 5. **a** Grating cell simulation in TiViPE. The three display icons yield input image, grating cell operator responses, and grayscale input image with grating responses (*red*) as illustrated in the next two figures. **b** Parameter settings of "GratingResponses," our implemented grating cell operator

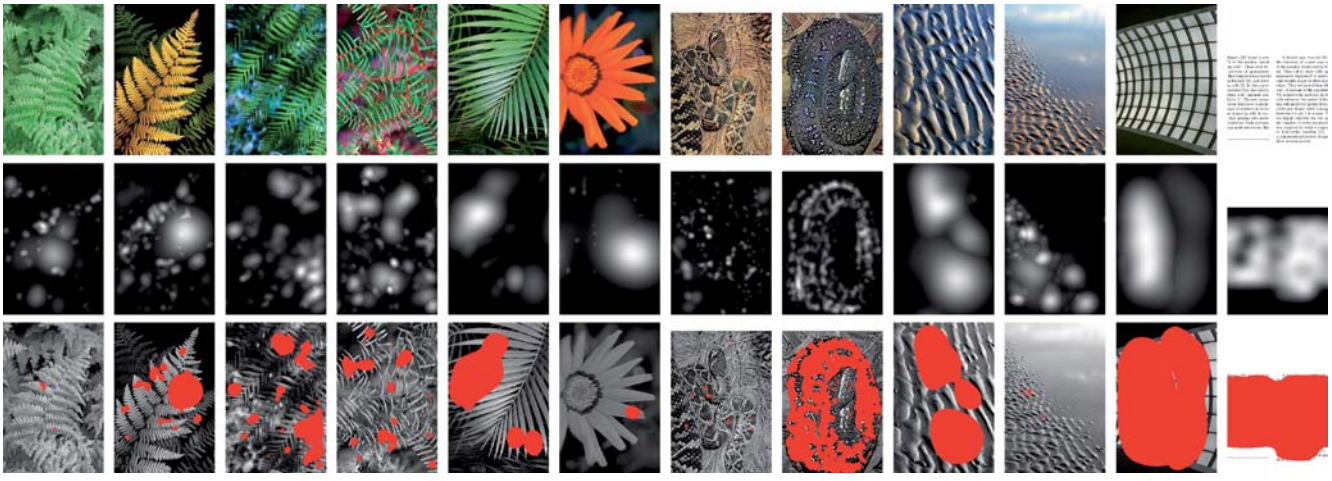

Fig. 6. Images of repetitive patterns (*first row*). Respective responses of the proposed grating cell operator. The results are normalized for better visualization; *white* denotes strong response, *black* no response (*second row*). Thresholded results (set to 7 where the response of the operator is between 0 and 255) in *red* as image overlay (*third row*)

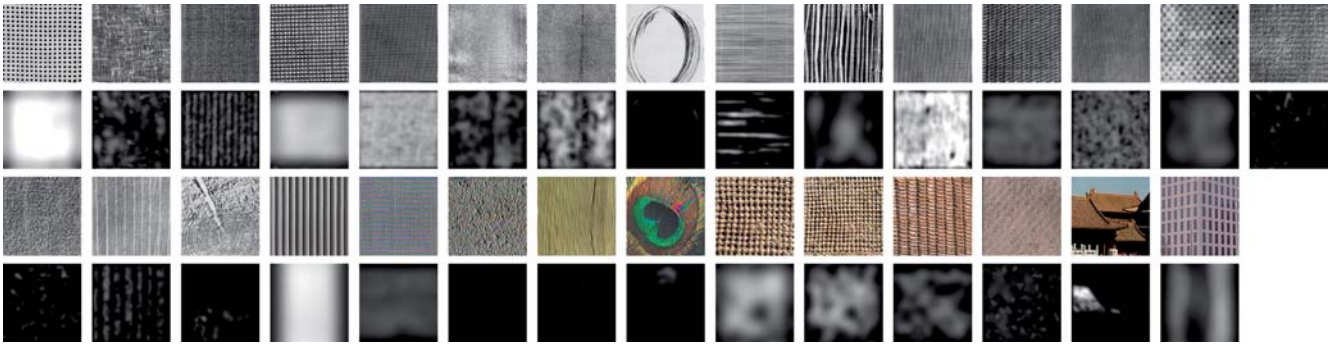

Fig. 7. Images from different databases (*odd rows*) and their response profiles as defined in (16), (*even rows*)

The grating cell operator was very selective and responded in only 5 (samples 38, 46, 49, 51, and 57) images in the ColumbiaUtrecht database and to 32 images of the Brodatz database. With the VisTex database the operator responded to 3 out of 18 categories of images (buildings, fabric, and tile), and within these categories it responded to about half of the images.

Figure 7 presents examples. These results suggest that cortical grating cells may respond well to the surface textures of human-made objects that include oriented periodic patterns.

6 Conclusions

In this paper, we presented a new model of cortical grating cells that produces response profiles similar to that of monkey grating cells (von der Heydt et al. 1992). Unlike previous models of grating cells (von der Heydt et al. 1991; Kruizinga and Petkov 1995; Petkov and Kruizinga 1997), the new model accounts for accurate spatial frequency tuning.

The model of Kruizinga and Petkov (1999) is an oriented texture operator since it responds well to oriented texture. The model is inspired by cortical grating cells, but response profiles differ rather strongly from that of these cortical cells.

Brunner et al. (1998) proposed a neural network model for the emergence of grating cells. The model considers developmental issues and activity-dependent self-organization and is from this perspective attractive. However, the results do not closely resemble the responses of cortical grating cells. For instance, this model is moderately orientation sensitive (the half-maximum response is around $\pm 30^\circ$, in contrast to the highly orientation-sensitive cortical grating cells where the half-maximum response is at $\pm 6^\circ$). The model showed similarities in response to the numbers of bars but did not demonstrate how cells developed to different preferred spatial frequencies, nor were other characteristics of cortical grating cells demonstrated.

Our model was applied to 49 different images with repetitive patterns from nature such as ferns, flowers, and animals as suggested by De Valois and De Valois (1988) and to 338 real-world images of textures from three databases. The results of these simulations show that the grating cell operators respond to oriented textures that include periodic patterns but are insensitive to many other textures. These patterns occur frequently in human-made patterns, but regular natural periodic patterns are relatively rare in nature.

The grating cell operator responds well if the complex cell responses perpendicular to the preferred orientation show similar strong responses. In such cases it is impossible to detect or extract relevant edges in these areas by using complex cells, since they respond to all locations of these grating patterns. We conclude, therefore, that cortical grating cells play a key role in separating form from texture, for example by giving inhibitory feedback to complex cells. Comparing a complex cell response that is strongly inhibited by grating cell responses demonstrates, upon first impression, similar results to the bar operator proposed by Petkov and Kruizinga (1997). However, the bar operator fully inhibits the overall grating pattern, while in our case the positions where the grating pattern begins and ends are not inhibited, nor are the positions where the gratings themselves end. In this respect the form of an object that contains a grating pattern is preserved, as demonstrated by Lourens et al. (2003). The positions where the gratings end are less uniform, but this could be compensated for by the so-called end-stopped type of grating cells, which were found by von der Heydt et al. (1992) as well.

Acknowledgements. The authors would like to thank Dr. E. Peterhans, the editor, and referees for many valuably comments and suggestions on the manuscript.

References

Albrecht D, De Valois RL, Thorell L (1980) Visual cortical neurons: are bars or gratings the optimal stimuli? Science 207:88–90

Andrews BW, Pollen DA (1979) Relationship between spatial frequency selectivity and receptive field profile of simple cells. J Physiol 287:163–176

Bauer C, Burger T, Lang EW (1999) A neural network model for the self-organization of cortical grating cells. In: Mira J, Sánchez-Andrés JV (eds) Foundations and tools for neural modeling. Proceedings of international work-conference on artificial and natural neural networks (IWANN'99), vol I. Alicante, 2–4 June 1999. Lecture notes in computer science, vol 1606. Springer, Berlin Heidelberg New York, pp 431–441

Brunner K, Kussinger M, Stetter M, Lang EW (1998) A neural network model for the emergence of grating cells. Biol Cybern 78:389–397

Daugman JG (1985) Uncertainty relation for resolution in space, spatial frequency, and orientation optimized by two-dimensional visual cortical filters. J Opt Soc Am 2(7):1160–1169

De Valois RL, Albrecht D, Thorell L (1978) Cortical cells: bar and edge detectors, or spatial frequency filters. In: Cool S, III ES (eds) Frontiers of visual Science. Springer, Berlin Heidelberg New York

De Valois KK, De Valois RL, Yund E (1979) Responses of striate cortical cells to grating and checkerboard patterns. J Physiol Lond 291:483–505

De Valois RL, De Valois KK (1988) Spatial vision. Oxford University Press, Oxford

Engel S, Zhang X, Wandell B (1997) Colour tuning in human visual cortex measured with functional magnetic resonance imaging. Nature 388:68–71

Gegenfurther KR, Kiper DC, Fenstemaker SB (1996) Processing of color, form, and motion in macaque area v2. Vis Neurosci 13:161–172

Hubel D, Wiesel T (1962) Receptive fields, binocular interaction, and functional architecture in the cat's visual cortex. J Physiol Lond 160:106–154

Hubel D, Wiesel T (1974) Sequence regularity and geometry of orientation columns in the monkey striate cortex. J Comp Neurol 154:106–154

Jones J, Palmer L (1987) An evaluation of the two-dimensional gabor filter model of simple receptive fields in cat striate cortex. J Neurophysiol 58:1233–1258

Kaplan E, Shapley RM (1986) The primate retina contains two types of ganglion cells, with high and low contrast sensitivity. Proc Natl Acad Sci USA 83:2755–2757

Kruizinga P, Petkov N (1995) A computational model of periodic-pattern-selective cells. In: Mira J, Sandoval F (eds) Proceedings of the international workshop on artificial neural networks (IWANN'95). Lecture notes in computer science, vol 930. Springer Berlin Heidelberg New York, pp 90–99

Kruizinga P, Petkov N (1999) Nonlinear operator for oriented texture. IEEE Trans Image Process 8(10):1395–1407

Livingstone MS, Hubel DH (1984) Anatomy and physiology of a color system in the primate visual cortex. J Neurosci 4:309–356

Lourens T (1998) A biologically plausible model for corner-based object recognition from color images. Shaker, Maastricht

Lourens T, Barakova EI, Tsujino H (2003) Interacting modalities through functional brain modeling. In: Mira J, Álvarez JR (eds) Proceedings of the international work-conference on artificial and natural neural networks (IWANN'03). Lecture notes in computer science, vol 2686, Springer, Berlin Heidelberg New York, pp 102–109

Morrone MC, Burr DC (1988) Feature detection in human vision: a phase-dependent energy model. Proc R Soc Lond 235:335–354

Movshon JA, Thompson ID, Tolhurst DJ (1978) Receptive field organization of complex cells in the cat's striate cortex. J Physiol 283:53–77

Petkov N, Kruizinga P (1997) Computational models of visual neurons specialised in the detection of periodic and aperiodic oriented visual stimuli: bar and grating cells. Biol Cybern 76(2):83–96

Tamura H, Sato H, Katsuyama N, Hata Y, Tsumoto T (1996) Less segregated processing of visual information in v2 than in v1 of the monkey visual cortex. Eur J Neurosci 8:300–309

von der Heydt R (1987) Approaches to visual cortical function. In: Reviews of physiology biochemistry and pharmacology, vol 108. Springer, Berlin Heidelberg New York, pp 69–150

von der Heydt R, Peterhans E, Dürsteler MR (1991) Grating cells in monkey visual cortex: coding texture? Visual cortex. In: Blum B (ed) Channels in the visual nervous system: neurophysiology, psychophysics and models. Freund, London, pp 53–73

von der Heydt R, Peterhans E, Dürsteler MR (1992) Periodic-pattern-selective cells in monkey visual cortex. J Neurosci 12(4):1416–1434

Würtz RP, Lourens T (2000) Corner detection in color images through a multiscale combination of end-stopped cortical cells. Image Vis Comput 18(6–7):531–541

Zeki S (1993) A vision of the brain. Blackwell, London